

Measurement-assisted non-Gaussian gate for Schrödinger cat states preparation: Fock resource state versus cubic phase state

A. V. Baeva,¹ N. G. Veselkova,² N. I. Masalaeva,³ and I. V. Sokolov^{1,*}

¹*Saint Petersburg State University, 7/9 Universitetskaya nab., Saint Petersburg, 199034 Russia*

²*Peter the Great St.Petersburg Polytechnic University (SPbPU),*

St.Petersburg, Polytechnicheskaya, 29, 195251, Russia

³*Institut für Theoretische Physik, Universität Innsbruck, Technikerstraße 21a, A-6020 Innsbruck, Austria*

In this paper, we consider the preparation of Schrödinger cat states using a measurement-assisted gate based on the Fock resource state, the quantum non-demolition (QND) entangling operation, and the homodyne measurement. Previously we have investigated the gate, which for the same goal uses the ancillary non-Gaussian cubic phase state generated from quadrature squeezed states at realistic (finite) squeezing. It is of evident interest to compare the efficiency of both schemes, that is, their ability to produce cat-like superpositions with high fidelity and probability of success. We introduce, in parallel with the exact theoretical description of the gate operation, a clear visual interpretation of the output state based on the semiclassical mapping of the input field variables. The emergence of the superpositions of “copies” of the input state in both schemes is due to the fact that such mapping is compatible with two (or, in general, more) sets of values of the output field observables. We demonstrate that even fine details of the output of both gates are effectively predicted and interpreted in our approach. We examine the fidelity and success probability and reveal the ranges of physical parameters where the Fock state-based and the cubic phase state-based gates demonstrate comparable fidelity and (or) probability of success.

I. INTRODUCTION

Modern quantum technologies require to go beyond the domain of Gaussian states and introduce the non-Gaussian elements [1]. The non-Gaussian states and non-Gaussian operations [2–6] are crucial for a variety of quantum information processing protocols [7] related to quantum key distribution [8–11], entanglement distillation [12–14], quantum error correction [15–19], quantum metrology [20–26], optimal cloning [27], continuous variable (CV) quantum computing [28–30], and quantum computation on cluster states [31, 32]. In addition, the non-Gaussian states and operations have been shown to be capable of improving the quality of entanglement [33] and enhancing the accuracy of CV quantum teleportation [34–40].

The CV Gaussian and non-Gaussian measurement-induced quantum networks are rapidly developing fields of quantum information science and technologies including optical quantum computing [41], methods for building neural networks on quantum computers [42], and secure quantum communication [43, 44]. Optical CV entangled quantum networks [45] that allow to simulate complex network structures [46, 47], including quantum communication in the global-scale quantum internet [48, 49], are an essential resource for measurement-based quantum protocols. To perform quantum protocols, such networks should make use of the non-Gaussian statistics.

Due to their importance in quantum information science and technology, the non-Gaussian states, such as Fock states [50–53], Schrödinger-cat states [54–57], NOON states [58, 59], and the non-Gaussian operations including photon-number subtraction and addition [37, 60–66], the Kerr nonlinearity [67], cubic-phase gate [68, 69], sum-frequency generation [70], photon-added Gaussian channels [71], and other operations [72] are

being intensively studied theoretically and implemented experimentally [73].

It is common to call a superposition of macroscopically (classically) distinguishable states of an object [74, 75] a Schrödinger cat state. In quantum optics, a Schrödinger cat state is usually related to a superposition of coherent states of an electromagnetic field and is a non-Gaussian state. The cat-like quantum superpositions have been of particular interest since the creation of quantum theory: they serve as a resource for the tests of the foundations of quantum mechanics [76–78] and also play a substantial role in up-to-date quantum technologies, including quantum information processing [54, 79–81] and quantum computing [28, 82–85], quantum communication and quantum repeaters [86–88], quantum teleportation [89], etc., as well as the measurements with non-classical states of light [90].

The generation of large-amplitude coherent-state superpositions ($|\alpha| \geq 2$) attracts significant practical interest [79, 82, 91] since such cat states can be used as a basis for preparing qubits in CV quantum computation [82, 85], and as a resource for quantum coding with error correction [17–19].

In general, CV Schrödinger cat states can be prepared through a strong enough nonlinear interaction using unitary evolution [92]. However, the development of realistic schemes for preparing optical Schrödinger cat states with a large number of photons and controlled quantum characteristics is still a challenging task. A variety of well-established approaches were proposed for this goal, including the schemes based on photon-number subtraction [93–97], quantum state engineering [98–101], iterative growth methods [102–105], etc. To date, the most successful optical method seems to be the application of intense laser fields to atomic gas to generate the desired non-classical states of light [106–109]. By using this approach the cat state containing $\langle n \rangle \approx 9.4$ photons was generated in the experiment [109], which is the largest optical cat state by now. Therefore, proposals for the production of Schrödinger cat states with the use of the non-Gaussian resource states and

* i.sokolov@mail.spbu.ru, sokolov.i.v@gmail.com

measurement are an actual alternative to the other cat-states generation methods.

In previous papers [110–112], we proposed a CV measurement-induced two-node logical gate using a QND entangling operation and a cubic phase state as a resource, which conditionally generate a Schrödinger cat state. An advantage of this scheme is that the output cat state can be a superposition of two well-spaced on the phase plane “copies” of the initial state of the target oscillator.

If Gaussian resource state of the ancilla oscillator is replaced with a non-Gaussian one, like the Fock state [55, 102] or the cubic phase state [110–112], the result of the measurement of the auxiliary oscillator can be compatible not with one, but with two (or, in general, more) different values of the physical variables of the target oscillator. This feature does not appear in Gaussian quantum networks and is crucial for preparing the Schrödinger cat states. The production of optical Schrödinger cat states using a photon number state as a resource, a beamsplitter as an entangling element, and a homodyne detection was experimentally demonstrated in a low-photon regime [55, 102].

In this paper, we discuss the preparation of Schrödinger cat states using a measurement-assisted gate based on the Fock resource state, the QND entangling operation, and the homodyne measurement. We compare this scheme with the gate that uses the cubic phase state as a non-Gaussian resource [112] to create a cat-like state. We discuss the similarities and differences between both gates and demonstrate that even fine details of the output state of both schemes are effectively predicted and interpreted not only by an exact theoretical description but also by a visual interpretation in terms of a semiclassical in-out mapping of the quadrature amplitudes of two oscillators. We consider the fidelity and success probability for both schemes, and reveal the ranges of physical parameters where these gates demonstrate comparable efficiencies.

II. ENGINEERING CAT-LIKE STATES USING FOCK STATES AS A NON-GAUSSIAN RESOURCE

The proposed scheme for producing cat states is depicted in Fig. 1. The input state of the target oscillator can be arbitrary with the wave function in the coordinate representation

$$|\psi_1\rangle = \int dx_1 \psi^{(in)}(x_1) |x_1\rangle, \quad (1)$$

while the ancillary oscillator is prepared in the Fock state with n photons

$$|\psi_2\rangle = \int dx_2 \psi^{(n)}(x_2) |x_2\rangle, \quad (2)$$

where

$$\psi^{(n)}(x_2) = \frac{1}{\pi^{1/4} \sqrt{2^n n!}} H_n(x_2) e^{-x_2^2/2}. \quad (3)$$

Here $H_n(x_2)$ is the Hermite polynomial.

Note that as far as the semiclassical mapping described below does not depend on the input state of the target oscillator and

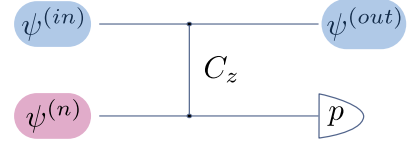


Figure 1. Schematic of the protocol for producing cat states using an ancilla oscillator in the Fock state. The states $\psi^{(in)}$ and $\psi^{(n)}$ of the target and ancillary oscillators are sent to the input of the scheme. After applying the C_z entangling operation, the ancilla momentum is measured by a homodyne detector. Depending on the measurement outcome y_m , the target oscillator state collapses to a cat-like state $\psi^{(out)}$.

works for a wide range of input states that occupy a limited area on the phase plane, the gate operation is not limited to the vacuum state at the input.

After applying the C_Z entangling operator $\exp(iq_1 q_2)$ to the oscillators, the resulting wave function takes the form

$$|\psi_{12}\rangle = \frac{1}{\pi^{1/4} \sqrt{2^n n!}} \int dx_1 dx_2 \psi^{(in)}(x_1) H_n(x_2) e^{ix_1 x_2} \times e^{-x_2^2/2} |x_1\rangle |x_2\rangle. \quad (4)$$

The momentum of ancilla is measured by the homodyne detector with the measurement outcome y_m , and the output wave function of the target oscillator is

$$\psi^{(out)}(x, y_m) = \frac{1}{\sqrt{N}} \psi^{(in)}(x) [F\psi^{(n)}](y_m - x), \quad (5)$$

where $x_1 \rightarrow x$ for brevity, N is the normalization factor, and F denotes the Fourier transform,

$$[F\psi](y) \equiv \frac{1}{\sqrt{2\pi}} \int dx e^{-iyx} \psi(x). \quad (6)$$

The Fourier transform of the Fock state of ancilla is given by

$$\begin{aligned} [F\psi^{(n)}](y) &= \frac{1}{\sqrt{2\pi}} \int dx e^{-iyx} \psi^{(n)}(x) = (-i)^n \psi^{(n)}(y) \\ &= \frac{(-i)^n}{\pi^{1/4} \sqrt{2^n n!}} H_n(y) e^{-y^2/2}, \end{aligned} \quad (7)$$

and we arrive at the output wave function of our gate,

$$\psi^{(out)}(x, y_m) = \frac{1}{\sqrt{N}} \tilde{\psi}^{(out)}(x, y_m). \quad (8)$$

Here $\tilde{\psi}^{(out)}(x, y_m)$ is the non-normalized output wave function collapsed by the measurement,

$$\begin{aligned} \tilde{\psi}^{(out)}(x, y_m) &= \psi^{(in)}(x) \\ &\times \frac{(-i)^n}{\pi^{1/4} \sqrt{2^n n!}} H_n(y_m - x) e^{-(y_m - x)^2/2}. \end{aligned} \quad (9)$$

As it will be demonstrated later, the considered above scheme produces at the output a superposition of two copies of the initial state of the target oscillator, by analogy with the gate using an ancilla oscillator in the cubic phase state [110–112]. Since the superpositions of coherent states are widely considered as a tool for the error correction schemes, and as a logical basis for computational operations [82, 85], in the following we will focus on the vacuum initial state of the target oscillator.

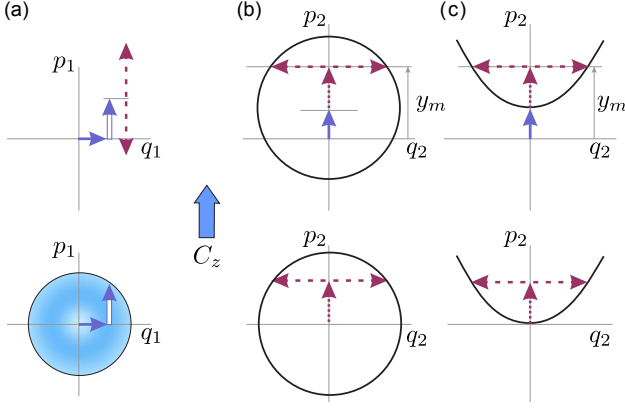


Figure 2. The measurement-induced semiclassical mapping of the quadrature amplitudes of the target [(a) column] and ancilla oscillators [(b) and (c) columns]. Here, column (b) represents the gate with the ancillary oscillator in the Fock state $\psi^{(n)}$, while column (c) corresponds to the gate with the ancillary oscillator prepared initially in a perfect cubic phase state. The randomly chosen initial amplitudes undergo the entangling non-demolition C_z operation, which transfers the target oscillator amplitudes to the ancilla and vice versa. The measurement of ancilla momentum with the outcome y_m [top row of (b) and (c) columns] specifies the values of the amplitudes compatible both with the preparation and the measurement. Since these amplitudes in both cases arise as multivalued, the target oscillator state collapses to a cat-like state [the top row of (a) column]. The parameters of both gates can be matched in such a way that the arising cat states may have similar spacing between the copies but different probabilities of success and fidelities of the state preparation.

III. SCHRÖDINGER CAT STATE GENERATION IN SEMICLASSICAL PICTURE

As we have already discussed in Ref. [110–112], for the gate using the cubic phase state as the non-Gaussian resource, the closest to the exact solution representation of the output state in the form of a cat-like superposition of two “copies” of the target state can be effectively evaluated in the semiclassical picture. For the Fock state-based gate, the semiclassical in-out mapping of the quadrature amplitudes of the target state is also easily accessed starting from the Heisenberg picture.

We define the coordinate q_i and momentum operators p_i as $a_i = (q_i + ip_i)/\sqrt{2}$, where $[q_i, p_i] = i$. As far as the initial ancilla state is the Fock state $|n\rangle$, we assume that the basic equation that specifies the Fock state

$$\frac{1}{2}(q_2^2 + p_2^2)|n\rangle = (n + \frac{1}{2})|n\rangle, \quad (10)$$

in the semiclassical approximation yields

$$(q_2^{(\text{in})})^2 + (p_2^{(\text{in})})^2 = 2n + 1.$$

The two-mode entangling QND operation $C_z \sim \exp(iq_1q_2)$ applied to the initial state of the oscillators performs the following transformation in the Heisenberg picture,

$$\begin{aligned} q_1' &= q_1^{(\text{in})}, & p_1' &= p_1^{(\text{in})} + q_2^{(\text{in})}, \\ q_2' &= q_2^{(\text{in})}, & p_2' &= p_2^{(\text{in})} + q_1^{(\text{in})}. \end{aligned}$$

The measurement of the ancillary oscillator momentum with the outcome y_m yields $p_2' \rightarrow y_m$ in the semiclassical approximation, and we arrive at $q_2' \rightarrow \pm\sqrt{2n+1 - (y_m - q_1^{(\text{in})})^2}$. The in-out semiclassical mapping of the target oscillator quadrature amplitudes takes the form

$$\begin{aligned} q_1^{(\text{out})} &= q_1^{(\text{in})}, \\ p_1^{(\text{out})} &= p_1^{(\text{in})} \pm \sqrt{2n+1 - (y_m - q_1^{(\text{in})})^2}. \end{aligned} \quad (11)$$

As one can see, two solutions for the momentum arise. The latter indicates that the output state of the gate is a superposition of two macroscopically distinguishable contributions - a cat-like state. The measurement adds to their momenta the quantities

$$\pm\delta p(x) = \pm\sqrt{2n+1 - (y_m - x)^2}, \quad (12)$$

where x stands for $q_1^{(\text{in})}$ for the shorthand. In order to find the corresponding components of the output wave function we conjecture, in analogy to Ref. [110–112], that for a given component of the target oscillator wave function the semiclassical factor added by the measurement can be defined as

$$\varphi_{\text{sc}}^{(\pm)}(x) \sim \sqrt{P^{(\pm)}(x)} \exp\left[\pm i \int dx \delta p(x)\right], \quad (13)$$

up to the phase factor that will be discussed later. Here $P^{(\pm)}(x)$ is the partial probability density of the measurement outcome y_m for a given x , and the exponential factor provides the displacement in momentum implied by Eq. (11).

Consider the semiclassical density distribution of the ancillary oscillator in the phase plane shifted by x along the momentum quadrature by the entangling C_z operation, as illustrated in Fig. 2(b),

$$P^{(\text{anc})}(q_2, p_2, x) = \frac{1}{\pi} \delta[(p_2 - x)^2 + q_2^2 - (2n + 1)],$$

where

$$\int dq_2 dp_2 P^{(\text{anc})}(q_2, p_2, x) = 1.$$

The probabilities $P^{(\pm)}(x)$ are defined through the overlap of $P^{(\text{anc})}(q_2, p_2, x)$ with the area on phase plane that corresponds to the measurement outcome y_m ,

$$\begin{aligned} P^{(+)}(x) + P^{(-)}(x) &\sim \int dq_2 dp_2 \delta(p_2 - y_m) P^{(\text{anc})}(q_2, p_2, x) \\ &= \frac{1}{\pi} \int dq_2 dp_2 \delta(p_2 - y_m) \delta[(p_2 - x)^2 + q_2^2 - (2n + 1)] \\ &= \frac{1}{\pi} \int dq_2 \delta\left\{[q_2 - \Delta(x)][q_2 + \Delta(x)]\right\} = \frac{1}{\pi \Delta(x)}. \end{aligned}$$

Here $\Delta(x) = \sqrt{2n+1 - (y_m - x)^2} > 0$ in the regime where the mapping shown in Fig. 2(b) is multivalued. If the coordinates of the target state are localized within some area, $|x| \leq \delta x$, one can expect a “good” cat state for such measurement outcomes, that $y_m \pm \delta x < \sqrt{2n+1}$, since for all x there

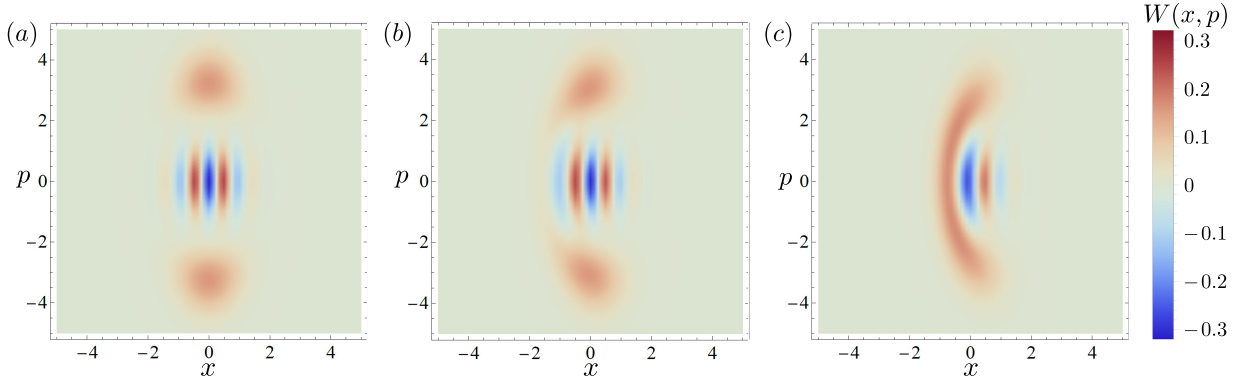


Figure 3. The Wigner function of the output state for the vacuum input state and the Fock resource state with $n = 5$ for different outcomes of the momentum measurements of ancilla: (a) $y_m = 0$, (b) $y_m = 1$, and (c) $y_m = 2$.

are two points of overlap, as depicted in Fig. 2(b). Note that $\Delta(x) = \delta p(x)$, hence,

$$P^{(\pm)}(x) \sim \frac{1}{|\delta p(x)|}. \quad (14)$$

By inserting (14) into (13), we arrive at a semiclassical added factor $\varphi_{\text{scl}}(x)$ that looks similar to the semiclassical wave function of a stationary state expressed through the momentum $\delta p(x)$. The superposition of semiclassical added factors, see Eq. (13), can be evaluated and written as

$$\varphi_{\text{scl}}(n, z) \sim \frac{1}{(1 - z^2)^{1/4}} [e^{i\phi(n, z)} + (-1)^n e^{-i\phi(n, z)}], \quad (15)$$

where

$$z = \frac{x - y_m}{\sqrt{2n + 1}}, \quad (16)$$

$$\phi(n, z) = \frac{1}{2}(2n + 1) \left(z\sqrt{1 - z^2} + \arcsin z \right).$$

The relative phase between two contributions $(-1)^n$ is chosen in accordance with the exact solution, see Eq. (9): for even n the added factor reaches a maximum at $x - y_m = 0$, and for odd n it is equal to 0.

To be specific, consider the action of the gate on the vacuum input state. An approximate version of Eq. (15) arises when the wave function of the input state is concentrated in a relatively small area of coordinate near $x = 0$. Assuming the denominator in (15) to be constant and Taylor expanding the phase $\phi(n, z)$ up to a linear term in the coordinate x , we receive

$$\phi(n, z) \approx \theta + p^{(+)}x + \dots, \quad (17)$$

where

$$\theta = \phi(n, -y_m/\sqrt{2n + 1}), \quad p^{(+)} = \sqrt{2n + 1 - y_m^2}. \quad (18)$$

In the limit $y_m \rightarrow 0$ one has $\theta \rightarrow 0$. As seen from Eq. (15), when the measured momentum of the ancilla oscillator is small, one can expect an even/odd cat-like output superposition depending on the number of photons in the resource state.

For the vacuum input state $\psi^{(0)}(x)$, the displaced component $\exp(ip^{(+)}x)\psi^{(0)}(x)$ of the output state is the Glauber coherent state $|\alpha\rangle$, where $\alpha = ip^{(+)}/\sqrt{2}$.

The approximations made up to now (that is, the semiclassical picture and linearization) yield the gate output state in the form of a superposition of two symmetrically displaced along the momentum axis coherent states,

$$|\psi^{(\text{coh})}\rangle = \frac{1}{\sqrt{\mathcal{N}_{\text{vac}}}} (e^{i\theta}|\alpha\rangle + (-1)^n e^{-i\theta}|\alpha\rangle), \quad (19)$$

where the normalization factor is

$$\mathcal{N}_{\text{vac}} = 2[1 + (-1)^n \cos(2\theta)e^{-2|\alpha|^2}].$$

Note that the relative phase θ for an arbitrary measurement outcome may acquire values that do not correspond to an even or odd cat state.

In the coordinate representation, the state (19) looks like

$$\psi^{(\text{coh})}(x, y_m) = \frac{\sqrt{2}}{\pi^{1/4}} \frac{\cos(\theta + p^{(+)}x)}{\sqrt{1 + \cos(2\theta)\exp(-p^{(+)^2})}} e^{-x^2/2}, \quad (20)$$

for the even n 's, and

$$\psi^{(\text{coh})}(x, y_m) = i \frac{\sqrt{2}}{\pi^{1/4}} \frac{\sin(\theta + p^{(+)}x)}{\sqrt{1 - \cos(2\theta)\exp(-p^{(+)^2})}} e^{-x^2/2}, \quad (21)$$

for the odd ones respectively. As can be seen from Eq. (19), for the optimal measurement outcome $y_m = 0$, when $\theta = 0$, the even or odd cat state can be produced as far as the approximations made in the semiclassical picture are valid.

In the following, we will evaluate fidelity between the exact form of the output state, see Eq. (9), and the even/odd cat state derived above. The latter will help us to match the output state with a “perfect” even/odd superposition of coherent states.

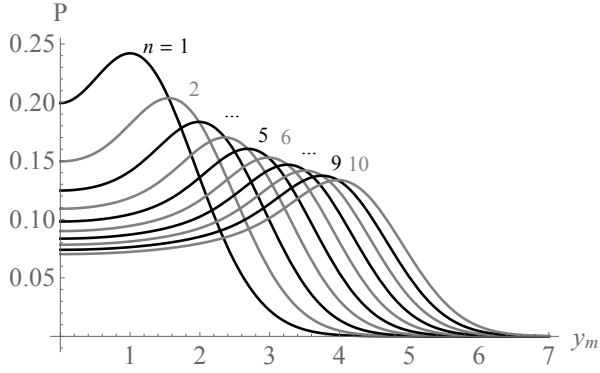


Figure 4. The probability density P as a function of the ancilla momentum measurement outcome y_m for the Fock resource states with $n = 1, 2, \dots, 10$ photons.

IV. WIGNER FUNCTION OF CAT STATES

The Wigner function of the exact output state (9) is given by

$$\begin{aligned}
 W^{(\text{out})}(x, y) &= \frac{1}{\pi} \int dz \psi^{(\text{out})*}(x+z, y_m) \psi^{(\text{out})}(x-z, y_m) \\
 &\times e^{2iyz} = \frac{1}{\pi N} \int dz \psi^{(\text{in})*}(x+z) \psi^{(\text{in})}(x-z) \\
 &\times [F\psi^{(n)}]^*(y_m - (x+z)) [F\psi^{(n)}](y_m - (x-z)) e^{2iyz}.
 \end{aligned} \quad (22)$$

In Fig. 3 we present a set of the Wigner functions of the output state in dependence on the measured ancilla momentum y_m for the vacuum input state of the target oscillator, $\psi^{(\text{in})}(x) = \psi^{(0)}(x)$. The ancilla oscillator is chosen to be in the Fock state with $n = 5$, which for the optimal measurement outcome, $y_m = 0$, provides the displacements of the copies equal to $\pm\sqrt{2n+1} \approx \pm 3.32$.

For the measurement outcome $y_m = 0$, the measurement-induced momentum displacements in the output state, see Eq. (12), are almost independent of the position x of the initial point, chosen within the support region of the target oscillator in the phase plane. In other words, for $y_m = 0$, the mapping is almost insensible to small shifts along the momentum axis of the circle that represents the resource Fock state for a large enough number of photons, due to its geometrical shape, see Fig. 1(b). As a result, one can expect a superposition of two “good” copies of the target state at the output of the scheme. As can be seen from Fig. 3(a), the Wigner function of the output state given by Eq. (22) for $y_m = 0$ is in good agreement with the above discussion.

For large enough measurement outcomes y_m , the copies of the input state of the target oscillator suffer from a shearing deformation of the opposite sign, see Fig. 3(b), due to almost linear dependence of displacements on x . For the even larger y_m , the two copies merge, as shown in Fig. 3(c), since for such measurement outcomes $\Delta(x) \leq 0$, and, as a consequence, two crossings of the circle, see Fig. 2(b), no longer exist for some x .

It is also clear from the developed above qualitative picture

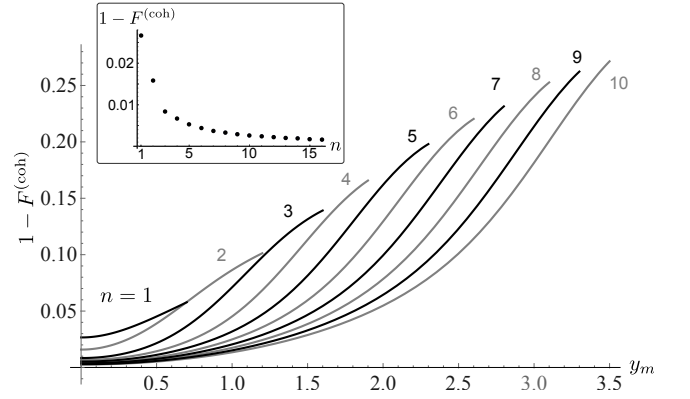


Figure 5. Infidelity $1 - F^{(\text{coh})}$ between the exact solution for the output state [Eq. (9)] and the corresponding superposition of two undistorted coherent states [Eq. (19)] as a function of the measurement outcome y_m . Here, the target oscillator is initially prepared in the vacuum state, and ancilla oscillator is in the Fock state with $n = 1, 2, \dots, 10$ photons. For every n , the infidelity is plotted within the range of positive y_m satisfying the condition $\Delta(x) > 0$, where one can expect a fair output cat state as it follows from the visual interpretation of the gate performance, see Fig. 2. We plot the infidelity for $y_m \geq 0$ only, since it is an even function of y_m . The inset shows the infidelity $1 - F^{(\text{coh})}$ as a function of the number of photons in the resource state n for the measurement outcome $y_m = 0$. As can be seen from the plot, such measurement outcome provides the highest fidelity.

that one can generate even/odd superpositions with high fidelities out of an arbitrary target state using the Fock resource states with the large enough dimensions of the uncertainty region (that is, with a large enough number of quanta) in comparison with the target state, which makes this cat state generating gate universal.

V. PROBABILITY VERSUS FIDELITY

The probability density to observe the measurement outcome y_m is given by the norm of the collapsed wave function (9),

$$P(y_m) = \langle \tilde{\psi}^{(\text{out})} | \tilde{\psi}^{(\text{out})} \rangle = \int dx |\tilde{\psi}^{(\text{out})}(x)|^2. \quad (23)$$

For the vacuum input state of the target oscillator and the Fock resource state with n photons, the probability density can be rewritten as

$$P(y_m) = \frac{1}{\pi 2^n n!} \int dx |H_n(y_m - x)|^2 e^{-(y_m - x)^2} e^{-x^2}, \quad (24)$$

and is shown in Fig. 4 for different measurement outcomes.

In order to evaluate how close is the output state [Eq. (8)] to a superposition of two coherent states, we consider two measures. The first one is the fidelity between the exact output state and the cat-like superposition (19), where the relative phase θ , given by Eq. (18), provides the best match to the exact solution but in general does not correspond to an even/odd cat state,

$$F^{(\text{coh})} = \left| \int dx \psi^{(\text{out})*}(x, y_m) \psi^{(\text{coh})}(x, y_m) \right|^2. \quad (25)$$

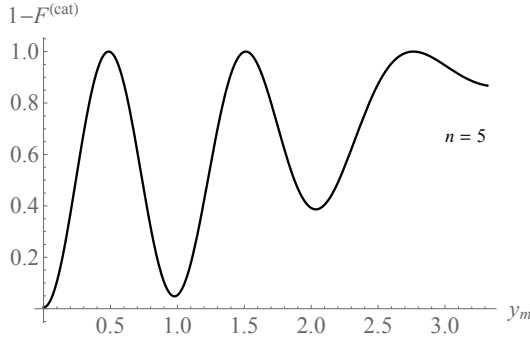


Figure 6. Infidelity $1 - F^{(\text{cat})}$ between the exact solution for the output cat state (9) and the corresponding odd cat state for the vacuum input state and the resource state with photon number $n = 5$ (21) as a function of the measurement outcome y_m .

The corresponding dependence of the infidelity $1 - F^{(\text{coh})}$ on the measurement outcome is shown in Fig. 5. For the optimal measurement result $y_m = 0$ the infidelity is depicted in more detail in the inset of Fig. 5.

As seen from Fig. 5, for any n the best fidelity is achieved for $y_m = 0$ where the distortion of copies is minimal, as it follows from the semiclassical picture. The Wigner functions presented in Fig. 3 for $n = 5$ also agree with this conclusion.

The dependence of the fidelity on n , shown in the inset of Fig. 5, demonstrates that with the increase of the photon number of ancilla, the gate, based on the Fock resource state, can produce superpositions of undistorted coherent states with high fidelities.

Since some error correction protocols rely on the even/odd superpositions of coherent states [19, 113], we plot in Fig. 6 the infidelity $1 - F^{(\text{cat})}$ between the odd cat state, which is given by Eq. (21), for $n = 5$ and optimal measurement outcome (that is, for $y_m = 0$ and $\theta = 0$), and the output state (9), when the observed ancilla momentum is not optimal,

$$F^{(\text{cat})} = \left| \int dx \psi^{(\text{out})*}(x, y_m) \psi^{(\text{coh})}(x, 0) \right|^2. \quad (26)$$

As the measured momentum y_m increases, the fidelity $F^{(\text{cat})}$ (for both even and odd n 's) degrades rapidly due to the evolution of the relative phase between the copies (18), which no longer matches the criterion $\theta = 0$. Hence, this is mostly a phase effect.

In order to increase the probability of the cat state preparation, one can introduce an acceptance interval $-d/2, d/2$ of width d for the measured ancilla momentum, centered at $y_m = 0$. In this case, a mixed state arises as the gate output. The weighted fidelity between the even/odd cat state and the mixed output state is evaluated as

$$F^{(\text{mix})}(d) = \frac{1}{P^{(\text{mix})}(d)} \int_{-d/2}^{+d/2} dy_m P(y_m) F^{(\text{cat})}(y_m). \quad (27)$$

Here

$$P^{(\text{mix})}(d) = \int_{-d/2}^{+d/2} dy_m P(y_m),$$

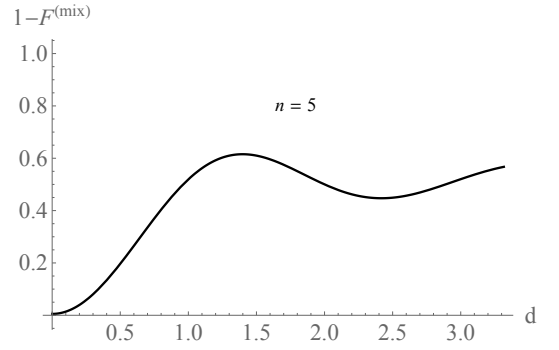


Figure 7. Infidelity $1 - F^{(\text{mix})}$, see Eq. (27), between the output mixed state and the target odd cat state as a function of the acceptance interval d .

is the probability that the measurement outcome will fit the acceptance interval. For the resource state with $n = 5$ photons, the infidelity $1 - F^{(\text{mix})}$ is shown in Fig. 7. For a small enough acceptance interval, $d \ll \sqrt{2n+1}$, the probability $P^{(\text{mix})}(d)$ is evaluated as $P^{(\text{mix})} \sim P(y_m \rightarrow 0) \times d$. This follows from the weak dependence of the probability density on y_m within the interval where the fidelity is high.

VI. FOCK RESOURCE STATE VERSUS CUBIC PHASE STATE

In this section, we compare the efficiency of the gate described above with the previously investigated scheme [110–112], which uses the cubic phase state as the non-Gaussian resource instead of the Fock state. It is instructive to discuss both gates by illustrating the similarities and differences between both schemes. Their visual representation is shown in Fig. 2, where the columns (b) and (c) represent the semiclassical mapping using the Fock resource state and cubic phase state, respectively. If the latter one is prepared from a perfectly squeezed state through quantum evolution with cubic Hamiltonian, its semiclassical support region can be depicted as a parabola.

Since both gates use the same QND operation to entangle the target and the ancillary oscillator, the mutual exchange of quadrature amplitudes looks similar in both devices. The gate based on the cubic phase state is described by a multivalued semiclassical mapping of the form [111]

$$\begin{aligned} q_1^{(\text{out})} &= q_1^{(\text{in})}, \\ p_1^{(\text{out})} &= p_1^{(\text{in})} \pm (3\gamma)^{-1/2} \sqrt{y_m - q_1^{(\text{in})} - p_2^{(\text{in})}}, \end{aligned} \quad (28)$$

which can be derived following the same steps as in the case of the Fock resource state. Here γ is the coupling parameter of the evolution operator $\exp(-i\gamma q_2^3)$ used for the preparation of cubic phase state, and $p_2^{(\text{in})}$ is the ancilla momentum before the application of the cubic deformation operator.

Similar to Eqs. (11), two solutions arise, which indicates that the output state is a superposition of two macroscopically distinguishable contributions - a cat-like state. The difference

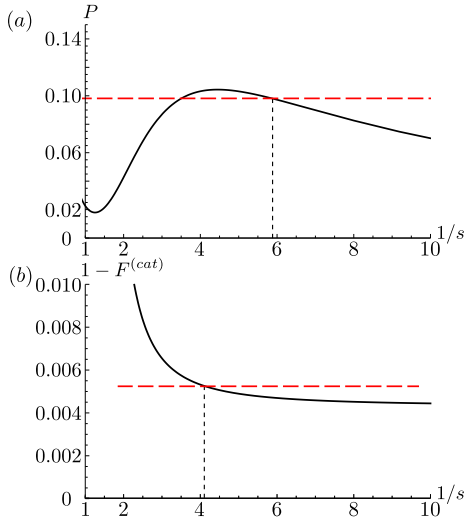


Figure 8. Fitting the inverse squeezing parameter $1/s$ of the ancilla oscillator for the cubic phase state-based gate to match the probability density $P = 0.098$ [(a), red dashed line], and infidelity $1 - F^{(\text{cat})} = 0.005$ [(b), red dashed line] for the Fock state-based gate used here for comparison. The gate using the cubic phase state achieves the same probability density (a), or the fidelity (b) for $\gamma = 0.075$, $y_m = 2.486$, $s = 0.171$, or $\gamma = 0.334$, $y_m = 11.012$, $s = 0.241$, respectively.

in the geometrical shapes of the semiclassical support regions for two resource states, evident from Fig. 2, manifests itself in different sensitivity of the output quadrature amplitudes, see Eqs. (11) and (28), to the choice of position of the initial point $\{q_1^{(\text{in})}, p_1^{(\text{in})}\}$ within the target oscillator support region, and, hence, in different distortion of the copies.

As we have already discussed, the Fock state-based gate prepares a cat-like state such that the spacing between the copies is determined by the number of quanta in the resource state and the momentum measurement outcome y_m , where minimal distortion takes place for $y_m = 0$. In order to put in correspondence the output state of the gate based on the cubic phase state, one has to estimate the proper values of the following parameters: (i) the parameter γ of cubic nonlinearity; (ii) the measurement outcome of the momentum of the ancillary oscillator y_m ; and (iii) the factor $s \leq 1$ of initial squeezing of the ancilla momentum before the cubic deformation is applied.

For the vacuum input state of the target oscillator and perfect initial squeezing, $s \rightarrow 0$, the spacing between the centers of copies is estimated from Eq. (28) by setting $q_1^{(\text{in})} \rightarrow 0$ and $p_2^{(\text{in})} \rightarrow 0$, which gives for the displacement of the copies $\pm p^{(+)} = \pm \sqrt{y_m/(3\gamma)}$. To achieve the same spacing between the copies of the input state of the target oscillator as for the discussed above Fock state-based gate with $n = 5$, where $\pm p^{(+)} = \pm \sqrt{2n+1} = \pm \sqrt{11}$, we accept such measurement outcomes, that $y_m = 33\gamma$.

It can be shown, see Ref. [111, 112], that the even/odd cat states represented by (19), where the phase θ is set to 0, arise for a discrete set of values of the pairs $\{y_m, \gamma\}$. Table I shows the values that correspond to the odd cat state similar to one produced by the Fock state-based gate for $n = 5$, $y_m = 0$.

y_m	γ
1.066	0.032
2.486	0.075
3.907	0.118
5.328	0.161
6.749	0.205
8.170	0.248
9.591	0.291
11.012	0.334
12.432	0.377

Table I. Values of the parameter γ of the cubic nonlinearity and the ancilla momentum measurement outcome y_m that correspond to the odd output cat state with the same displacement of copies along the momentum axis as for the Fock state-based gate considered above.

The Fock state-based gate at $n = 5$ and $y_m = 0$ produces the odd cat state with the probability density $P = 0.098$ and the fidelity $F^{(\text{cat})}$ such that $1 - F^{(\text{cat})} = 0.005$ (see Figs. 4 and 5, respectively).

The gate that uses the cubic phase state provides the same or better probability density for $\gamma = 0.075$, $y_m = 2.486$, see Table I, within some range of the ancilla coordinate stretching factor $1/s$, as shown in Fig. 8(a). The best fidelity $F^{(\text{cat})}$, such that $1 - F^{(\text{cat})} = 0.098$, is achieved by the maximal squeezing within this range, which corresponds to $s = 0.171$, or ~ 15 dB of squeezing [112].

Thus, in this particular example, for the gate with the Fock resource state, the infidelity is as much as by the order of magnitude less than with the cubic phase state. This difference is easily explained in terms of semiclassical visualization. By choosing for mapping an initial coordinate of the target oscillator on the phase plane, represented by a solid blue arrow in Fig. 2(a), one shifts the parabola, as shown on the top row of column (c). This changes the spacing between the two cross-sections that represent the measurement procedure and eventually leads to the distortion of copies. As one can observe from (28) and from the visual representation in Fig. 2(c), the distortion of copies due to the parabolic shape of the ancilla support region becomes smaller for larger cubic nonlinearity γ , so that two branches of the parabola become closer to vertical. The chosen value of the cubic nonlinearity $\gamma = 0.075$ is not enough to meet this criterion.

To achieve the same fidelity as with the Fock resource state, $1 - F^{(\text{cat})} = 0.005$, one can choose from Table I the gate parameters, that correspond to the larger cubic nonlinearity. The first suitable choice is $\gamma = 0.334$, $y_m = 11.012$. Note that a non-perfect squeezing introduces some noise and also may affect the fidelity. For the chosen values of $\{\gamma, y_m\}$, the infidelity in dependence on the squeezing parameter is shown in Fig. 8(b). The minimal squeezing compatible with the given above value of the fidelity corresponds to $s = 0.241$, or ~ 12 dB of squeezing. The gain in fidelity is achieved at the expense of the probability density, $P = 0.022$, which is smaller than the corresponding one $P = 0.098$ for the Fock resource state.

The Wigner functions of the output states of the gates that we have compared above are shown in Fig. 9. These plots are in agreement with the qualitative picture and its visualization

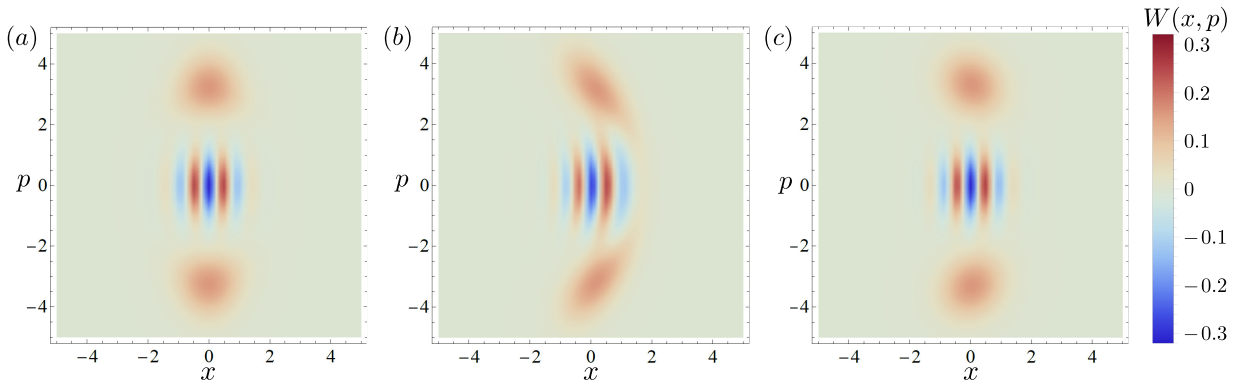


Figure 9. Wigner functions of the output cat-like states of the gates that use vacuum input state and the considered above non-Gaussian resource states: (a) the Fock resource state with $n = 5$ and optimal measurement outcome $y_m = 0$ that corresponds to the odd cat state with the displacement of the copies $\pm p^{(+)} = \pm 3.32$, the probability density $P = 0.098$, and the infidelity $1 - F^{(cat)} = 0.005$; (b) the cubic phase state with the parameters $\gamma = 0.075$, $y_m = 2.486$ chosen in such way that the gate has the same probability density of the measurement outcome as in the case (a); (c) the cubic phase state with the parameters $\gamma = 0.075$, $y_m = 2.486$ that provide the same infidelity as in the case (a).

presented here.

VII. CONCLUSION

In this paper, we have shown that the gate using the Fock resource state demonstrates better overall efficiency in producing the cat-like states in terms of fidelity and probability of success in comparison with the gate based on the cubic phase state. The latter one provides a comparable fidelity at the expense of probability, and to be competitive needs rather large cubic nonlinearity, which is evident from a simple geometrical picture. On the other hand, in order to produce the odd/even cat states, the Fock resource states with the odd/even numbers of quanta should be used, which corresponds to different spacing between the copies and could be not suitable for some schemes of error correction. In the case of the resource cubic phase state, a fixed cubic nonlinearity can be used, while the relative phase between the components of the cat state is specified

by accepting the suitable measurement outcome of the ancilla momentum [111, 112]. For the gate parameters that provide a comparable fidelity, the spacing between the copies is less dependent on the measurement outcome.

Using our approach to the analysis of different non-Gaussian measurement-assisted gates, one can in some cases easily assess such important features as the distortions introduced by the gate to the output states, the fidelity, the probability of success, etc., with a simple geometrical description based on the semiclassical mapping, including the “shape” of the resource state, the entanglement, and the measurement.

ACKNOWLEDGMENTS

A. V. B. acknowledges financial support from the Theoretical Physics and Mathematics Advancement Foundation “BASIS” (Grant No. XXXXXX)

-
- [1] M. Walschaers, Non-Gaussian quantum states and where to find them, *PRX Quantum* **2**, 030204 (2021).
 - [2] T. J. Bartley and I. A. Walmsley, Directly comparing entanglement-enhancing non-Gaussian operations, *New Journal of Physics* **17**, 023038 (2015).
 - [3] T. J. Bartley, P. J. D. Crowley, A. Datta, J. Nunn, L. Zhang, and I. Walmsley, Strategies for enhancing quantum entanglement by local photon subtraction, *Phys. Rev. A* **87**, 022313 (2013).
 - [4] L. Hu, M. Al-amri, Z. Liao, and M. S. Zubairy, Entanglement improvement via a quantum scissor in a realistic environment, *Phys. Rev. A* **100**, 052322 (2019).
 - [5] Y. Mardani, A. Shafiei, M. Ghadimi, and M. Abdi, Continuous-variable entanglement distillation by cascaded photon replacement, *Phys. Rev. A* **102**, 012407 (2020).
 - [6] J. Liu, Y. Maleki, and M. S. Zubairy, Optimal entanglement enhancing via conditional measurements, *Phys. Rev. A* **105**, 062405 (2022).
 - [7] Q. Zhuang, P. W. Shor, and J. H. Shapiro, Resource theory of non-Gaussian operations, *Phys. Rev. A* **97**, 052317 (2018).
 - [8] Y. Guo, W. Ye, H. Zhong, and Q. Liao, Continuous-variable quantum key distribution with non-Gaussian quantum catalysis, *Phys. Rev. A* **99**, 032327 (2019).
 - [9] W. Ye, H. Zhong, Q. Liao, D. Huang, L. Hu, and Y. Guo, Improvement of self-referenced continuous-variable quantum key distribution with quantum photon catalysis, *Optics Express* **27**, 17186 (2019).
 - [10] C. Kumar, J. Singh, S. Bose, and Arvind, Coherence-assisted non-Gaussian measurement-device-independent quantum key distribution, *Phys. Rev. A* **100**, 052329 (2019).
 - [11] L. Hu, M. Al-amri, Z. Liao, and M. S. Zubairy, Continuous-variable quantum key distribution with non-Gaussian operations, *Phys. Rev. A* **102**, 012608 (2020).
 - [12] S. L. Braunstein and P. van Loock, Quantum information with continuous variables, *Rev. Mod. Phys.* **77**, 513 (2005).

- [13] C. Weedbrook, S. Pirandola, R. García-Patrón, N. J. Cerf, T. C. Ralph, J. H. Shapiro, and S. Lloyd, Gaussian quantum information, *Rev. Mod. Phys.* **84**, 621 (2012).
- [14] G. Adesso, S. Ragy, and A. R. Lee, Continuous variable quantum information: Gaussian states and beyond, *Open Systems & Information Dynamics* **21**, 1440001 (2014).
- [15] J. Niset, J. Fiurášek, and N. J. Cerf, No-go theorem for Gaussian quantum error correction, *Phys. Rev. Lett.* **102**, 120501 (2009).
- [16] N. Ofek, A. Petrenko, R. Heeres, P. Reinhold, Z. Leghtas, B. Vlastakis, Y. Liu, L. Frunzio, S. M. Girvin, L. Jiang, M. Mirrahimi, M. H. Devoret, and R. J. Schoelkopf, Extending the lifetime of a quantum bit with error correction in superconducting circuits, *Nature* **536**, 441 (2016).
- [17] H. M. Vasconcelos, L. Sanz, and S. Glancy, All-optical generation of states for “encoding a qubit in an oscillator”, *Optics Letters* **35**, 3261 (2010).
- [18] D. J. Weigand and B. M. Terhal, Generating grid states from Schrödinger-cat states without postselection, *Phys. Rev. A* **97**, 022341 (2018).
- [19] J. Hastrup, J. S. Neergaard-Nielsen, and U. L. Andersen, Deterministic generation of a four-component optical cat state, *Optics Letters* **45**, 640 (2020).
- [20] R. Birrittella, J. Mimihi, and C. C. Gerry, Multiphoton quantum interference at a beam splitter and the approach to Heisenberg-limited interferometry, *Phys. Rev. A* **86**, 063828 (2012).
- [21] R. Carranza and C. C. Gerry, Photon-subtracted two-mode squeezed vacuum states and applications to quantum optical interferometry, *Journal of the Optical Society of America B* **29**, 2581 (2012).
- [22] D. Braun, P. Jian, O. Pinel, and N. Treps, Precision measurements with photon-subtracted or photon-added Gaussian states, *Phys. Rev. A* **90**, 013821 (2014).
- [23] Y. Ouyang, S. Wang, and L. Zhang, Quantum optical interferometry via the photon-added two-mode squeezed vacuum states, *Journal of the Optical Society of America B* **33**, 1373 (2016).
- [24] H. Zhang, W. Ye, C. Wei, Y. Xia, S. Chang, Z. Liao, and L. Hu, Improved phase sensitivity in a quantum optical interferometer based on multiphoton catalytic two-mode squeezed vacuum states, *Phys. Rev. A* **103**, 013705 (2021).
- [25] J. Joo, W. J. Munro, and T. P. Spiller, Quantum metrology with entangled coherent states, *Phys. Rev. Lett.* **107**, 083601 (2011).
- [26] A. Facon, E.-K. Dietsche, D. Grosso, S. Haroche, J.-M. Raimond, M. Brune, and S. Gleyzes, A sensitive electrometer based on a Rydberg atom in a Schrödinger-cat state, *Nature* **535**, 262 (2016).
- [27] N. J. Cerf, O. Krüger, P. Navez, R. F. Werner, and M. M. Wolf, Non-Gaussian cloning of quantum coherent states is optimal, *Phys. Rev. Lett.* **95**, 070501 (2005).
- [28] S. Lloyd and S. L. Braunstein, Quantum computation over continuous variables, *Phys. Rev. Lett.* **82**, 1784 (1999).
- [29] S. D. Bartlett and B. C. Sanders, Universal continuous-variable quantum computation: Requirement of optical nonlinearity for photon counting, *Phys. Rev. A* **65**, 042304 (2002).
- [30] A. Mari and J. Eisert, Positive Wigner functions render classical simulation of quantum computation efficient, *Phys. Rev. Lett.* **109**, 230503 (2012).
- [31] M. Ohliger, K. Kieling, and J. Eisert, Limitations of quantum computing with Gaussian cluster states, *Phys. Rev. A* **82**, 042336 (2010).
- [32] N. C. Menicucci, P. van Loock, M. Gu, C. Weedbrook, T. C. Ralph, and M. A. Nielsen, Universal quantum computation with continuous-variable cluster states, *Phys. Rev. Lett.* **97**, 110501 (2006).
- [33] C. Navarrete-Benlloch, R. García-Patrón, J. H. Shapiro, and N. J. Cerf, Enhancing quantum entanglement by photon addition and subtraction, *Phys. Rev. A* **86**, 012328 (2012).
- [34] T. Opatrny, G. Kurizki, and D.-G. Welsch, Improvement on teleportation of continuous variables by photon subtraction via conditional measurement, *Phys. Rev. A* **61**, 032302 (2000).
- [35] Y. Yang and F.-L. Li, Entanglement properties of non-Gaussian resources generated via photon subtraction and addition and continuous-variable quantum-teleportation improvement, *Phys. Rev. A* **80**, 022315 (2009).
- [36] X.-x. Xu, Enhancing quantum entanglement and quantum teleportation for two-mode squeezed vacuum state by local quantum-optical catalysis, *Phys. Rev. A* **92**, 012318 (2015).
- [37] S. Wang, L.-L. Hou, X.-F. Chen, and X.-F. Xu, Continuous-variable quantum teleportation with non-Gaussian entangled states generated via multiple-photon subtraction and addition, *Phys. Rev. A* **91**, 063832 (2015).
- [38] L. Hu, Z. Liao, and M. S. Zubairy, Continuous-variable entanglement via multiphoton catalysis, *Phys. Rev. A* **95**, 012310 (2017).
- [39] C. Kumar and S. Arora, Success probability and performance optimization in non-Gaussian continuous-variable quantum teleportation, *Phys. Rev. A* **107**, 012418 (2023).
- [40] E. R. Zinatullin, S. B. Korolev, and T. Y. Golubeva, Teleportation protocols with non-Gaussian operations: Conditional photon subtraction versus cubic phase gate, *Phys. Rev. A* **107**, 022422 (2023).
- [41] S. Takeda and A. Furusawa, Universal quantum computing with measurement-induced continuous-variable gate sequence in a loop-based architecture, *Phys. Rev. Lett.* **119**, 120504 (2017).
- [42] N. Killoran, T. R. Bromley, J. M. Arrazola, M. Schuld, N. Quesada, and S. Lloyd, Continuous-variable quantum neural networks, *Phys. Rev. Res.* **1**, 033063 (2019).
- [43] J. Lee, J. Park, and H. Nha, Quantum non-Gaussianity and secure quantum communication, *npj Quantum Information* **5**, 49 (2019).
- [44] Y. Guo, Q. Liao, Y. Wang, D. Huang, P. Huang, and G. Zeng, Performance improvement of continuous-variable quantum key distribution with an entangled source in the middle via photon subtraction, *Phys. Rev. A* **95**, 032304 (2017).
- [45] M. Walschaers, B. Sundar, N. Treps, L. D. Carr, and V. Parigi, Emergent complex quantum networks in continuous-variables non-Gaussian states, *Quantum Science and Technology* **8**, 035009 (2023).
- [46] J. Nokkala, F. Arzani, F. Galve, R. Zambrini, S. Maniscalco, J. Piilo, N. Treps, and V. Parigi, Reconfigurable optical implementation of quantum complex networks, *New Journal of Physics* **20**, 053024 (2018).
- [47] F. Sansavini and V. Parigi, Continuous variables graph states shaped as complex networks: Optimization and manipulation, *Entropy* **22**, 26 (2019).
- [48] Y. Cai, J. Roslund, G. Ferrini, F. Arzani, X. Xu, C. Fabre, and N. Treps, Multimode entanglement in reconfigurable graph states using optical frequency combs, *Nature Communications* **8**, 15645 (2017).
- [49] F. Arzani, G. Ferrini, F. Grosshans, and D. Markham, Random coding for sharing bosonic quantum secrets, *Phys. Rev. A* **100**, 022303 (2019).
- [50] A. Ourjoumtsev, R. Tualle-Brouiri, and P. Grangier, Quantum homodyne tomography of a two-photon Fock state, *Phys. Rev. Lett.* **96**, 213601 (2006).
- [51] M. Cooper, L. J. Wright, C. Söller, and B. J. Smith, Experimental generation of multi-photon Fock states, *Optics Express* **21**, 5309 (2013).

- [52] M. Bouillard, G. Boucher, J. F. Ortas, B. Kanseri, and R. Tualle-Brouri, High production rate of single-photon and two-photon Fock states for quantum state engineering, *Optics Express* **27**, 3113 (2019).
- [53] J. Tiedau, T. J. Bartley, G. Harder, A. E. Lita, S. W. Nam, T. Gerrits, and C. Silberhorn, Scalability of parametric down-conversion for generating higher-order Fock states, *Phys. Rev. A* **100**, 041802 (2019).
- [54] A. Ourjoumtsev, R. Tualle-Brouri, J. Laurat, and P. Grangier, Generating optical Schrödinger kittens for quantum information processing, *Science* **312**, 83 (2006).
- [55] A. Ourjoumtsev, H. Jeong, R. Tualle-Brouri, and P. Grangier, Generation of optical ‘Schrödinger cats’ from photon number states, *Nature* **448**, 784 (2007).
- [56] N. Quesada, L. G. Helt, J. Izaac, J. M. Arrazola, R. Shahrokshahi, C. R. Myers, and K. K. Sabapathy, Simulating realistic non-Gaussian state preparation, *Phys. Rev. A* **100**, 022341 (2019).
- [57] K. Takase, J.-i. Yoshikawa, W. Asavanant, M. Endo, and A. Furusawa, Generation of optical Schrödinger cat states by generalized photon subtraction, *Phys. Rev. A* **103**, 013710 (2021).
- [58] A. N. Boto, P. Kok, D. S. Abrams, S. L. Braunstein, C. P. Williams, and J. P. Dowling, Quantum interferometric optical lithography: Exploiting entanglement to beat the diffraction limit, *Phys. Rev. Lett.* **85**, 2733 (2000).
- [59] H. Lee, P. Kok, and J. P. Dowling, A quantum Rosetta stone for interferometry, *Journal of Modern Optics* **49**, 2325 (2002).
- [60] V. Parigi, A. Zavatta, M. Kim, and M. Bellini, Probing quantum commutation rules by addition and subtraction of single photons to/from a light field, *Science* **317**, 1890 (2007).
- [61] J. Fiurášek, Engineering quantum operations on traveling light beams by multiple photon addition and subtraction, *Phys. Rev. A* **80**, 053822 (2009).
- [62] P. Marek, H. Jeong, and M. S. Kim, Generating “squeezed” superpositions of coherent states using photon addition and subtraction, *Phys. Rev. A* **78**, 063811 (2008).
- [63] A. Kitagawa, M. Takeoka, M. Sasaki, and A. Chefles, Entanglement evaluation of non-Gaussian states generated by photon subtraction from squeezed states, *Phys. Rev. A* **73**, 042310 (2006).
- [64] N. Namekata, Y. Takahashi, G. Fujii, D. Fukuda, S. Kurimura, and S. Inoue, Non-Gaussian operation based on photon subtraction using a photon-number-resolving detector at a telecommunications wavelength, *Nature Photonics* **4**, 655 (2010).
- [65] J. Fiurášek, R. García-Patrón, and N. J. Cerf, Conditional generation of arbitrary single-mode quantum states of light by repeated photon subtractions, *Phys. Rev. A* **72**, 033822 (2005).
- [66] K. Wakui, H. Takahashi, A. Furusawa, and M. Sasaki, Photon subtracted squeezed states generated with periodically poled KTiOPO₄, *Optics Express* **15**, 3568 (2007).
- [67] K. Nemoto and W. J. Munro, Nearly deterministic linear optical controlled-NOT gate, *Phys. Rev. Lett.* **93**, 250502 (2004).
- [68] D. Gottesman, A. Kitaev, and J. Preskill, Encoding a qubit in an oscillator, *Phys. Rev. A* **64**, 012310 (2001).
- [69] F. Arzani, N. Treps, and G. Ferrini, Polynomial approximation of non-Gaussian unitaries by counting one photon at a time, *Phys. Rev. A* **95**, 052352 (2017).
- [70] Q. Zhuang, Z. Zhang, and J. H. Shapiro, Optimum mixed-state discrimination for noisy entanglement-enhanced sensing, *Phys. Rev. Lett.* **118**, 040801 (2017).
- [71] K. K. Sabapathy and A. Winter, Non-Gaussian operations on bosonic modes of light: Photon-added Gaussian channels, *Phys. Rev. A* **95**, 062309 (2017).
- [72] J. Wenger, R. Tualle-Brouri, and P. Grangier, Non-Gaussian statistics from individual pulses of squeezed light, *Phys. Rev. Lett.* **92**, 153601 (2004).
- [73] B. Q. Baragiola, G. Pantaleoni, R. N. Alexander, A. Karanjai, and N. C. Menicucci, All-Gaussian universality and fault tolerance with the Gottesman-Kitaev-Preskill code, *Phys. Rev. Lett.* **123**, 200502 (2019).
- [74] S. Haroche, Nobel lecture: Controlling photons in a box and exploring the quantum to classical boundary, *Rev. Mod. Phys.* **85**, 1083 (2013).
- [75] F. Fröwis, P. Sekatski, W. Dür, N. Gisin, and N. Sangouard, Macroscopic quantum states: Measures, fragility, and implementations, *Rev. Mod. Phys.* **90**, 025004 (2018).
- [76] M. Brune, E. Hagley, J. Dreyer, X. Maître, A. Maali, C. Wunderlich, J. M. Raimond, and S. Haroche, Observing the progressive decoherence of the “meter” in a quantum measurement, *Phys. Rev. Lett.* **77**, 4887 (1996).
- [77] J. Wenger, M. Hafezi, F. Grosshans, R. Tualle-Brouri, and P. Grangier, Maximal violation of Bell inequalities using continuous-variable measurements, *Phys. Rev. A* **67**, 012105 (2003).
- [78] R. García-Patrón, J. Fiurášek, N. J. Cerf, J. Wenger, R. Tualle-Brouri, and P. Grangier, Proposal for a loophole-free Bell test using homodyne detection, *Phys. Rev. Lett.* **93**, 130409 (2004).
- [79] A. Gilchrist, K. Nemoto, W. J. Munro, T. C. Ralph, S. Glancy, S. L. Braunstein, and G. J. Milburn, Schrödinger cats and their power for quantum information processing, *Journal of Optics B: Quantum and Semiclassical Optics* **6**, S828 (2004).
- [80] B. Vlastakis, G. Kirchmair, Z. Leghtas, S. E. Nigg, L. Frunzio, S. M. Girvin, M. Mirrahimi, M. H. Devoret, and R. J. Schoelkopf, Deterministically encoding quantum information using 100-photon Schrödinger cat states, *Science* **342**, 607 (2013).
- [81] P. Jouguet, S. Kunz-Jacques, A. Leverrier, P. Grangier, and E. Diamanti, Experimental demonstration of long-distance continuous-variable quantum key distribution, *Nature Photonics* **7**, 378 (2013).
- [82] T. C. Ralph, A. Gilchrist, G. J. Milburn, W. J. Munro, and S. Glancy, Quantum computation with optical coherent states, *Phys. Rev. A* **68**, 042319 (2003).
- [83] A. P. Lund, T. C. Ralph, and H. L. Haselgrove, Fault-tolerant linear optical quantum computing with small-amplitude coherent states, *Phys. Rev. Lett.* **100**, 030503 (2008).
- [84] M. Mirrahimi, Z. Leghtas, V. V. Albert, S. Touzard, R. J. Schoelkopf, L. Jiang, and M. H. Devoret, Dynamically protected cat-qubits: a new paradigm for universal quantum computation, *New Journal of Physics* **16**, 045014 (2014).
- [85] P. T. Cochrane, G. J. Milburn, and W. J. Munro, Macroscopically distinct quantum-superposition states as a bosonic code for amplitude damping, *Phys. Rev. A* **59**, 2631 (1999).
- [86] P. van Loock, N. Lütkenhaus, W. J. Munro, and K. Nemoto, Quantum repeaters using coherent-state communication, *Phys. Rev. A* **78**, 062319 (2008).
- [87] N. Sangouard, C. Simon, N. Gisin, J. Laurat, R. Tualle-Brouri, and P. Grangier, Quantum repeaters with entangled coherent states, *Journal of the Optical Society of America B* **27**, A137 (2010).
- [88] R. Goncharov, A. D. Kiselev, F. Kiselev, E. S. Moiseev, E. Samsonov, S. A. Moiseev, and V. Egorov, *Quantum repeater via entangled phase modulated multimode coherent states* (2022), arXiv:2211.03597.
- [89] S. J. van Enk and O. Hirota, Entangled coherent states: Teleportation and decoherence, *Phys. Rev. A* **64**, 022313 (2001).
- [90] K. C. Tan and H. Jeong, Nonclassical light and metrological power: An introductory review, *AVS Quantum Science*

- 1, 014701 (2019).
- [91] I. A. Walmsley, Quantum optics: Science and technology in a new light, *Science* **348**, 525 (2015).
 - [92] B. Yurke and D. Stoler, Generating quantum mechanical superpositions of macroscopically distinguishable states via amplitude dispersion, *Phys. Rev. Lett.* **57**, 13 (1986).
 - [93] R. Dong, A. Tipsmark, A. Laghaout, L. A. Krivitsky, M. Ježek, and U. L. Andersen, Generation of picosecond pulsed coherent state superpositions, *Journal of the Optical Society of America B* **31**, 1192 (2014).
 - [94] T. Gerrits, S. Glancy, T. S. Clement, B. Calkins, A. E. Lita, A. J. Miller, A. L. Migdall, S. W. Nam, R. P. Mirin, and E. Knill, Generation of optical coherent-state superpositions by number-resolved photon subtraction from the squeezed vacuum, *Phys. Rev. A* **82**, 031802 (2010).
 - [95] W. Asavanant, K. Nakashima, Y. Shiozawa, J.-I. Yoshikawa, and A. Furusawa, Generation of highly pure Schrödinger's cat states and real-time quadrature measurements via optical filtering, *Optics Express* **25**, 32227 (2017).
 - [96] H. Takahashi, K. Wakui, S. Suzuki, M. Takeoka, K. Hayasaka, A. Furusawa, and M. Sasaki, Generation of large-amplitude coherent-state superposition via ancilla-assisted photon subtraction, *Phys. Rev. Lett.* **101**, 233605 (2008).
 - [97] J. S. Neergaard-Nielsen, M. Takeuchi, K. Wakui, H. Takahashi, K. Hayasaka, and M. Sasaki, Optical continuous-variable qubit, *Phys. Rev. Lett.* **105**, 053602 (2010).
 - [98] E. Bimbard, N. Jain, A. MacRae, and A. I. Lvovsky, Quantum-optical state engineering up to the two-photon level, *Nature Photonics* **4**, 243 (2010).
 - [99] M. Yukawa, K. Miyata, T. Mizuta, H. Yonezawa, P. Marek, R. Filip, and A. Furusawa, Generating superposition of up-to three photons for continuous variable quantum information processing, *Optics Express* **21**, 5529 (2013).
 - [100] A. E. Ulanov, I. A. Fedorov, D. Sychev, P. Grangier, and A. I. Lvovsky, Loss-tolerant state engineering for quantum-enhanced metrology via the reverse Hong–Ou–Mandel effect, *Nature Communications* **7**, 11925 (2016).
 - [101] K. Huang, H. Le Jeannic, J. Ruaudel, V. B. Verma, M. D. Shaw, F. Marsili, S. W. Nam, E. Wu, H. Zeng, Y.-C. Jeong, R. Filip, O. Morin, and J. Laurat, Optical synthesis of large-amplitude squeezed coherent-state superpositions with minimal resources, *Phys. Rev. Lett.* **115**, 023602 (2015).
 - [102] J. Etesse, M. Bouillard, B. Kanseri, and R. Tualle-Brouri, Experimental generation of squeezed cat states with an operation allowing iterative growth, *Phys. Rev. Lett.* **114**, 193602 (2015).
 - [103] D. V. Sychev, A. E. Ulanov, A. A. Pushkina, M. W. Richards, I. A. Fedorov, and A. I. Lvovsky, Enlargement of optical Schrödinger's cat states, *Nature Photonics* **11**, 379 (2017).
 - [104] A. P. Lund, H. Jeong, T. C. Ralph, and M. S. Kim, Conditional production of superpositions of coherent states with inefficient photon detection, *Phys. Rev. A* **70**, 020101 (2004).
 - [105] A. Laghaout, J. S. Neergaard-Nielsen, I. Rigas, C. Kragh, A. Tipsmark, and U. L. Andersen, Amplification of realistic Schrödinger-cat-state-like states by homodyne heralding, *Phys. Rev. A* **87**, 043826 (2013).
 - [106] T. Lamprou, I. Lontos, N. C. Papadakis, and P. Tzallas, A perspective on high photon flux nonclassical light and applications in nonlinear optics, *High Power Laser Science and Engineering* **8**, e42 (2020).
 - [107] M. Lewenstein, M. F. Ciappina, E. Pisanty, J. Rivera-Dean, P. Stammer, T. Lamprou, and P. Tzallas, Generation of optical Schrödinger cat states in intense laser–matter interactions, *Nature Physics* **17**, 1104 (2021).
 - [108] P. Stammer, J. Rivera-Dean, T. Lamprou, E. Pisanty, M. F. Ciappina, P. Tzallas, and M. Lewenstein, High photon number entangled states and coherent state superposition from the extreme ultraviolet to the far infrared, *Phys. Rev. Lett.* **128**, 123603 (2022).
 - [109] J. Rivera-Dean, T. Lamprou, E. Pisanty, P. Stammer, A. F. Ordóñez, A. S. Maxwell, M. F. Ciappina, M. Lewenstein, and P. Tzallas, Strong laser fields and their power to generate controllable high-photon-number coherent-state superpositions, *Phys. Rev. A* **105**, 033714 (2022).
 - [110] I. Sokolov, Schrödinger cat states in continuous variable non-Gaussian networks, *Physics Letters A* **384**, 126762 (2020).
 - [111] N. Masalaeva and I. Sokolov, Quantum statistics of Schrödinger cat states prepared by logical gate with non-Gaussian resource state, *Physics Letters A* **424**, 127846 (2022).
 - [112] A. Baeva, A. Losev, and I. Sokolov, Schrödinger cat states prepared by logical gate with non-Gaussian resource state: Effect of finite squeezing and efficiency versus monotones, *Physics Letters A* **466**, 128730 (2023).
 - [113] D. S. Schlegel, F. Minganti, and V. Savona, Quantum error correction using squeezed Schrödinger cat states, *Phys. Rev. A* **106**, 022431 (2022).